The Journal of Experimental Biology 208, 3075-3092
Published by The Company of Biologists 2005
doi:10.1242/jeb.01744

The aerodynamic effects of wing–wing interaction in flapping insect wings

Fritz-Olaf Lehmann[1,*], Sanjay P. Sane[2] and Michael Dickinson[3]

[1]*Biofuture Research Group, Department of Neurobiology, University of Ulm, 89069 Ulm, Germany*, [2]*Department of Biology, University of Washington, Seattle, WA 98195-1800, USA* and [3]*California Institute of Technology, MC 138-78, Pasadena, CA 91125, USA*

*Author for correspondence (e-mail: fritz.lehmann@uni-ulm.de)

Accepted 8 June 2005

Summary

We employed a dynamically scaled mechanical model of the small fruit fly *Drosophila melanogaster* (Reynolds number 100–200) to investigate force enhancement due to contralateral wing interactions during stroke reversal (the 'clap-and-fling'). The results suggest that lift enhancement during clap-and-fling requires an angular separation between the two wings of no more than 10–12°. Within the limitations of the robotic apparatus, the clap-and-fling augmented total lift production by up to 17%, but depended strongly on stroke kinematics. The time course of the interaction between the wings was quite complex. For example, wing interaction attenuated total force during the initial part of the wing clap, but slightly enhanced force at the end of the clap phase. We measured two temporally transient peaks of both lift and drag enhancement during the fling phase: a prominent peak during the initial phase of the fling motion, which accounts for most of the benefit in lift production, and a smaller peak of force enhancement at the end fling when the wings started to move apart. A detailed digital particle image velocimetry (DPIV) analysis during clap-and-fling showed that the most obvious effect of the bilateral 'image' wing on flow occurs during the early phase of the fling, due to a strong fluid influx between the wings as they separate. The DPIV analysis revealed, moreover, that circulation induced by a leading edge vortex (LEV) during the early fling phase was smaller than predicted by inviscid two-dimensional analytical models, whereas circulation of LEV nearly matched the predictions of Weis-Fogh's inviscid model at late fling phase. In addition, the presence of the image wing presumably causes subtle modifications in both the wake capture and viscous forces. Collectively, these effects explain some of the changes in total force and lift production during the fling. Quite surprisingly, the effect of clap-and-fling is not restricted to the dorsal part of the stroke cycle but extends to the beginning of upstroke, suggesting that the presence of the image wing distorts the gross wake structure throughout the stroke cycle.

Supplementary material available online at
http://jeb.biologists.org/cgi/content/full/208/16/3075/DC1

Key words: clap-and-fling, wake capture, wing–wake interaction, leading edge vortex LEV, robotic wing, digital particle image velocimetry, *Drosophila*.

Introduction

Whether circling flowers or pursuing prey, insects display a diverse variety of aerial maneuvers. These behaviors ultimately result from the animals' fine control over wing kinematics and the resulting aerodynamic forces. In recent times, the mechanisms of aerodynamic force production have been the subject of some rigorous theoretical and experimental investigations (for recent reviews, see Sane, 2003; Lehmann, 2004). In his classic paper on the aerodynamic mechanisms of the tiny wasp *Encarsia formosa*, Weis-Fogh (1973) described a novel 'clap-and-fling' pattern of wing motion occurring at dorsal stroke reversal. During the clap, the insect brings the leading edges of the two wings together, while pronating them until the 'v-shaped' gap vanishes and the wings are parallel in close apposition. During the fling, the wings pronate about their trailing edge, creating a growing gap as the leading edges pull part. As described for *E. formosa*, the two wings act essentially as rigid plates during this behavior. Since the first description by Weis-Fogh, many researchers have observed subtle variations in the exact motion of the wings during clap-and-fling (for a review, see Marden, 1987; see also Ennos, 1989; Wakeling, 1997). For example, in tethered flying *Drosophila* (Götz, 1987; Lehmann, 1994), various species of butterflies (Dalton, 1975; Ellington, 1984a; Brackenbury, 1991a; Brodsky, 1991), bush cricket, mantis (Brackenbury, 1990, 1991b), and locust (Cooter and Baker, 1977), the wings are curved along their chords and *peel* apart during the fling rather than rigidly flinging. In the white butterfly *Pieris barssicae*, the bluebottle *Calliphora vicina* and the flour moth *Ephista,* the wings approach at the dorsal stroke reversal

without physically touching during the clap, thus exhibiting a partial or near clap-and-fling (Ellington, 1984a; Ennos, 1989).

Obligate use of the clap-and-fling has only been observed in small insects (Ellington, 1984a; Ennos, 1989), suggesting that the behavior might be essential for adequate lift production in small insects operating at low Reynolds numbers. A noteworthy exception is the fruit fly *Drosophila melanogaster*, which rarely employs a clap-and-fling motion during free flight (Ennos, 1989; Fry et al., 2003) but frequently exhibits a complete clap-and-fling when flown under tethered conditions (Vogel, 1966; Götz, 1987; Zanker, 1990a; Lehmann, 1994). Larger insects may employ the behaviour while carrying loads (Marden, 1987), or performing power demanding flight turns (Cooter and Baker, 1977). Ellington (1984a) suggested that the lacewing *Chrysopa carnea* uses clap-and-fling, not only for lift augmentation, but also for steering and flight control. Marden's experiments (Marden, 1987) on various insects showed that insects generate approximately 25% more aerodynamic lift per unit flight muscle (mean, 79.2 N kg^{-1}) when they clap-and-fling than insects using conventional wing kinematics (mean, 59.4 N kg^{-1}), although these values were based on solely on an estimate of induced power requirements for flight. Tethered flying *Drosophila* exhibit a bilateral asymmetry in wing motion during the clap-and-fling during presentation of optomotor stimuli (Götz, 1987; Zanker, 1990b; Lehmann, 1994). Specifically, the fly may delay the pronation of the wing on the inner side of a visually induced turn by as much as 0.2 ms, possibly modifying the direction of flight force (Lehmann, 1994). Moreover, electrophysiogical stimulation of the second basalare muscle (M.b2) during flight has indicated that the delay in wing rotation during open-loop optomotor flight condition is due to a change in angle of attack rather than to a change in rotational speed (Lehmann, 1994).

While the research cited above documented the use of the clap-and-fling, other studies explored the underlying fluid mechanics of the behavior. Weis-Fogh suggested that the function of the fling is to strengthen the development of circulation at the beginning of the downstroke (Weis-Fogh, 1973; see also Lighthill, 1973). Such enhancement could come about by two, non-exclusive, mechanisms. First, a low-pressure region between the two wings might initially draw fluid over the dorsal surface of each wing, thus enhancing circulation at the onset of the downstroke. Second, as the wings approach each other closely, the net circulation around them drops to zero due to mutual annihilation of equal and opposite circulation around each wing. During the following fling, the close proximity of the trailing edges inhibits the creation of the starting vortices, because the conservation of zero circulation for the entire system (as required by Kelvin's Law) is fulfilled by the equal and opposite circulation of the two wings as they move apart. The diminished strength of starting vortices would minimize the retarded development of circulation following an impulsive start due to the Wagner effect (Wagner, 1925). Lighthill (1973) pointed out that this phenomenon could operate within an inviscid fluid.

Many researchers have studied the fling using analytical methods (Lighthill, 1973; Ellington, 1975; Edwards and Cheng, 1982) and physical models (Bennett, 1977; Maxworthy, 1979; Spedding and Maxworthy, 1986; Sunada et al., 1993). However, the effect of clap has received less attention. Based on tethered flight kinematics in *Drosophila*, Götz (1987) argued that the fluid ejected from the closing gap at the end of the clap produces a momentum jet that augments force production (see also Ellington, 1984b). More recently, numerical simulations on the entire clap-and-fling sequence in both three dimensions (Sun and Yu, 2003) and in two dimensions across a wide range of Reynolds numbers (Miller and Peskin, 2004, 2005) show that clap is likely to enhance lift. However, these conclusions have not been verified using physical measurements.

In this paper, we explore the fluid dynamic mechanisms underlying clap-and-fling in greater detail using a dynamically scaled two-winged flapper, which enables us to measure the time course of forces throughout the entire stroke, while simultaneously visualizing the resulting flow fields using digital particle image velocimetry. By systemically varying the angular distance between the two wings at the dorsal stroke reversal, we evaluate the aerodynamic effect of wing–wing interaction during clap-and-fling. Further, by varying the kinematics of the stroke, we examine how these effects were influenced by subtle changes in wing motion.

Materials and methods

The methods used in this study have been published elsewhere in greater detail (Dickinson et al., 1999; Sane and Dickinson, 2001; Maybury and Lehmann, 2004) and we provide only a brief description here. We modeled the clap-and-fling using two computer-controlled, dynamically scaled Plexiglas wings (left and right wing) programmed to flap back and forth in prescribed kinematic patterns. One wing was equipped with a force transducer that measured forces perpendicular and parallel to the wing. From the measured force and the angular position of the wing throughout the stroke cycle, we reconstructed lift and drag force using custom software routines in MATLAB (MathWorks, Inc., Natick, MA, USA). The Plexiglas' wings (wing length=25 cm) were immersed in a 2 m^3 (1 m×1 m×2 m) tank of mineral oil (density=0.88×10^3 kg m^{-3}; kinematic viscosity=115 cSt) and flapped at Reynolds numbers between 50 and 200, depending on the kinematics of each trial. The wings had an aspect ratio of approximately 1.9 and were shaped like a wing of the fruit fly *Drosophila melanogaster* Meigen.

Kinematics

The prescribed kinematic patterns were constructed using custom MATLAB routines in which various aspects of wing motion could be modified. All experiments were conducted using stroke kinematics of approximately 160° in stroke amplitude. Depending on the experiment, we varied: (1) the distance between the wings, (2) the Reynolds number (by

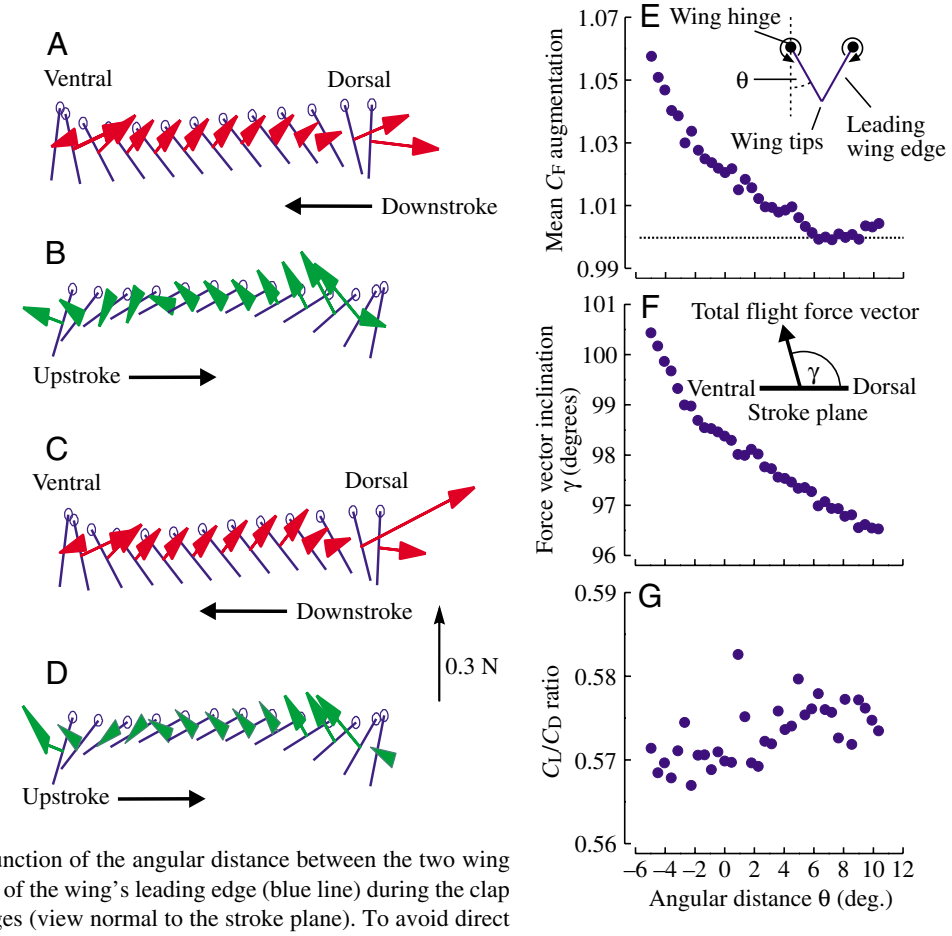

Fig. 1. Wing motion and force production of a robotic wing performing a clap-and-fling kinematic maneuver. (A–D) Diagrams of wing motion indicating magnitude and orientation of total force vector measured by a force transducer during the downstroke (red) and upstroke (green) of a dynamically scaled robotic model wing (stroke amplitude=160°; cycling frequency=0.16 Hz; geometrical angle of attack at midstroke=45°; wing shape similar to a *Drosophila* wing; mean Reynolds number is 134 and typical to *Drosophila* wing motion). Small circles at the beginning of each wing section (blue line) indicate the leading edge of the moving wing. The kinematic pattern was derived from kinematic data published for a tethered flying fruit fly *Drosophila* (Zanker, 1990a). The performance of flapping a single wing is shown in A and B. The vectors in C and D demonstrate forces produced by the wing when simultaneously flapping an imaged wing in close distance to promote the clap-and-fling maneuver at dorsal reversal. (E) Relative augmentation of the mean force vector coefficient due to the clap-and-fling wing beat, scaled to the performance of a single wing flapping. Data are plotted as a function of the angular distance between the two wing hinges. The pictogram illustrates the position of the wing's leading edge (blue line) during the clap and the location of the two robotic wing hinges (view normal to the stroke plane). To avoid direct mechanical stress on the force transducer, the wing tips do not physically touch during the clap phase. (F) Alterations of the mean force vector inclination with respect to the horizontal stroke plane when varying the angular distance between the two wings during the clap-and-fling maneuver. An angle of inclination greater than 90° indicates that the force vector points slightly into a ventral direction, which results in a pitching (nose) down moment. (G) The ratio between mean lift and drag coefficients (averaged over the entire stroke cycle) demonstrates how aerodynamic efficacy changes with decreasing angular distance of wing separation during dorsal stroke reversal.

changing the flapping frequency), or (3) rotational timing and angular velocity at the ventral and dorsal stroke reversal (for a description of kinematic angles, see Sane and Dickinson, 2001). In experiments investigating the effect of angular separation between the wings, we used a stroke pattern such that the mean geometric angle of attack at mid half stroke was 45°. In these patterns, wing rotation was symmetric about stroke reversal, with 4% of the wing rotation occurring before and 4% after stroke reversal. The wing kinematics of a tethered flying *Drosophila* were derived by slightly smoothing kinematic data published elsewhere (Zanker, 1990a). Throughout the paper we use the term 'angular distance' as the angle θ between the wing's spanwise or longitudinal axis and the mid plane between both robotic wings during clap-and-fling (defined in Lighthill, 1973; horizontal plane in Fig. 1). In contrast, the term 'total angular separation' between the wings is the total angle between the spanwise axes of both wings and thus twice the angular distance (2θ). In our robotic model, angular distance depends on two factors: the angular excursion of the wing in the stroke plane during dorsal wing rotation, and the distance between the two wing hinges. This is important because in one set of experiments, we added spacers between each wing and the corresponding wing hinge in order to minimize the gap between both wings during clap conditions. To simplify the comparison between the two sets of experiments (with and without spacers), we ignored the changes in θ due to the spacers and plotted all results against θ derived from experiments in which the wings were mounted without spacer in line with the rotational axis of the mechanical wing hinge. In general, there is no 'natural' or 'standard' clap-and-fling kinematic behavior for experimental modeling. Instead, the term clap-and-fling should be understood to be a whole set of kinematic patterns within a broad parameter space. This also includes modifications of the clap-and-fling due to wing elasticity ('peel') and fling motion following near-clap conditions.

Digital particle image velocimetry

To visualize wake structure during clap-and-fling, the oil was seeded with bubbles by pumping room air through a

ceramic water purification filter. The seeding consisted of approximately evenly sized bubbles at high concentration. After the bubbles had been generated, we waited for about 1 min to allow the larger bubbles to rise, thus minimizing the chances of getting spurious vertical flow due to rising bubbles. The smaller bubbles that remained in the fluid took approximately 15–20 min to rise to the top of the tank (Maybury and Lehmann, 2004). This small upward velocity was not detectable using the time delay settings of our measurements. To perform digital particle image velocimetry (DPIV) we used a TSI dual mini-Nd:YAG laser to create two identically positioned light sheets through the wing at five equally spaced distances from the wing base (wing base, 33%, 50% and 75% distance between wing base and tip, and a layer close to the wing tip) and an additional layer at the center of wing area at approximately 65% wing length (distance at which mean force vector acts on the *Drosophila* shaped wing; Birch and Dickinson, 2003). The paired images of approximately 185×185 mm^2 were captured at 12 different phases of the stroke cycle. Non-dimensional time within the stroke cycle, $\hat{t}$, is normalized as $\hat{t}=t/T$, where t is the time from the start of the downstroke and T is the stroke period. For convenience, when discussing the clap-and-fling, we will express non-dimensional time after the start of the downstroke as $\hat{t}+1$ (e.g. $\hat{t}=0.01=1.01$). Twelve sets of chordwise images were taken from the start of the clap to the end of the fling ($\hat{t}$=0.94, 0.97, 0.99, 1.00, 1.01, 1.02, 1.03, 1.05, 1.08. 1.10, 1.13 and 1.15). DPIV analysis on the velocity fields, including calculation of vorticity, was performed using TSI Insight v5.1 and TSI macros in Tecplot v9.0.

Translational force coefficients

We derived mean lift and drag coefficients, $\bar{C}_L$ and $\bar{C}_D$, respectively, for wing motion from mean lift and drag averaged throughout the entire stroke cycle using:

$$\bar{C}_L = \frac{8\bar{L}}{\rho\Phi^2 n^2 R^2 S\overline{(d\hat{\phi}/d\hat{t})^2}\hat{r}_2^2(S)}, \quad (1)$$

which is a modified expression of eq. 12 in Ellington (1984c), developed for hovering flying insects exhibiting a horizontal stroke plane (Lehmann and Dickinson, 1998). In this equation, $\bar{L}$ is lift of a single wing averaged throughout the stroke cycle, ρ is the density of the mineral oil, Φ is stroke amplitude defined as the angle that the wings cover during wing translation, n is stroke frequency, R is wing length, S is total wing area, $\overline{(d\hat{\phi}/d\hat{t})^2}$ is mean square of dimensionless wing velocity and $\hat{r}_2^2(S)$ is the non-dimensional radius of the second moment of wing area that characterizes wing shape (for nomenclature see Ellington, 1984d).

Fling coefficient

Weis-Fogh's kinematic two-dimensional (2-D) simplification of the clap-and-fling, based on his observations of *Encarsia Formosa* (Weis-Fogh, 1974), modeled the wings as rigid plates rotating around their trailing edges up to a separation angle of approximately 60° prior to the start of downstroke translation. In the present study, the Plexiglas wings are also essentially rigid and thus a blade-element version of Weis-Fogh's analytical model also applies to our experimental evaluation. According to 2-D inviscid flow theory, the fling induces circulation around each chordwise wing segment that depends on chord width, c, the angular rate of change of incidence of a single wing, ω, and a fling coefficient $\boldsymbol{g}(\theta)$ that describes the angle of the v-shaped wedge to which the wings open before they begin translating apart. If rotational motion is identical in both wings, the fling coefficient can be estimated experimentally from measured circulation as (Lighthill, 1973):

$$\boldsymbol{g}(\theta) = \Gamma_f c^{-2}\omega^{-1}. \quad (2)$$

In this equation Γ_f is the final circulation during fling motion for one wing and 2θ is the total gap angle between the wings at the end of the fling. Weis-Fogh originally defined Γ_f as the total circulation of both wings and in his equation ω is thus twice the rate of incidence change $2d\theta/dt$ (Weis-Fogh, 1973, 1974). The experimental evaluation of the clap-and-fling by Bennett (1977) follows Weis-Fogh's nomenclature. In contrast, Lighthill's analytical model on the contribution of vortex shedding defines ω as $d\theta/dt$, so that his circulation estimates are for a single wing (Lighthill, 1973). In this study we estimated the fling coefficient $\boldsymbol{g}(\theta)$ directly from our DPIV measurements and did not calculate $\boldsymbol{g}(\theta)$ from force measurements using a quasi-steady approach.

Results

Total force enhancement

The wing beat pattern of a tethered flying fruit fly *Drosophila* generates pronounced changes in total lift production during the clap-and-fling maneuver on the robotic wings. Fig. 1A,B shows a time sequence of one wing stroke cycle with superimposed instantaneous force vectors produced by an isolated single wing. In this case, the mean flight force normal to the wing surface and averaged throughout the entire stroke cycle is approximately 0.453 N, with a peak at the beginning of the downstroke of 1.34 N. In comparison, a wing undergoing the same kinematic pattern along with a second, mirror-image symmetric wing produces a mean force of approximately 0.476 N, with a peak of 1.82 N (Fig. 1C,D). In this experiment, the angular distance θ between the spanwise axis of each wing and the horizontal during the clap was –4.95° (inset, Fig. 1E). To investigate the significance of angular distance on mean flight force enhancement, we systemically varied θ during dorsal stroke in 0.45° steps (Fig. 1E). Maximum enhancement of normal force averaged throughout the entire stroke cycle (5.8% relative to the single wing case) occurred at an angular distance of –4.95 (–9.9° total angular separation), when the wings almost touch each other at the wing tips. The force enhancement due to the presence of an image wing is limited to a small angular distance between the wings, and completely vanishes when the angle exceeds values

of approximately 6° (exponential decay fit; $y=1.0+0.023e^{-x/5.25}$, $r^2=0.98$, $\chi^2/DF=5.91\times10^{-6}$, $N=35$). Due to the increase in force production at the beginning of the downstroke in the presence of an image wing, the mean flight force vector tilts slightly ventral (forward for a horizontal stroke plane) by approximately 4.0° from 96.5° at an angular distance between the wings of 10° to approximately 101° when the wings are closest during the clap (Fig. 1C,F). We found only small changes in the ratio between mean lift and drag coefficients (0.57 to 0.58) while varying the angular distance between the two wings (Fig. 1G).

Due to the alignment of the wing hinges and the rigidity of the robotic wings, the generic kinematic pattern that we used did not allow a full clap, in which both wings physically touch along their entire surface (Fig. 1A–D), so the wings are not parallel during the clap and the wing bases are farther apart than the wing tips (left insert, Fig. 2, inter-wing base distance ~4.3 cm). To investigate the potential significance of a wing clap with wings oriented parallel to each other, we added plastic spacers between the wing hinge and wing base to minimize the gap between the wings during the clap (right inset, Fig. 2, inter-wing base distance ~0.5 cm). To highlight the consequences of alterations in wing gap for lift production in the robotic model, Fig. 2 shows mean lift coefficient augmentation for wings with and without the spacers in place, plotted as functions of angular wing distance. In both cases, the lift coefficient steadily decreases with increasing wing separation (exponential decay fit; blue: $y=1.0+0.038e^{-x/5.5}$, $r^2=0.98$, $\chi^2/DF=1.4\times10^{-5}$, $N=35$; red: $y=0.99+0.12e^{-x/6.29}$, $r^2=0.93$, $\chi^2/DF=7.7\times10^{-5}$, $N=25$). The presence of spacers permits a parallel alignment during the clap, and further enhances lift by 3.9% (from 9.4% to 13.3%) relative to the one-wing case.

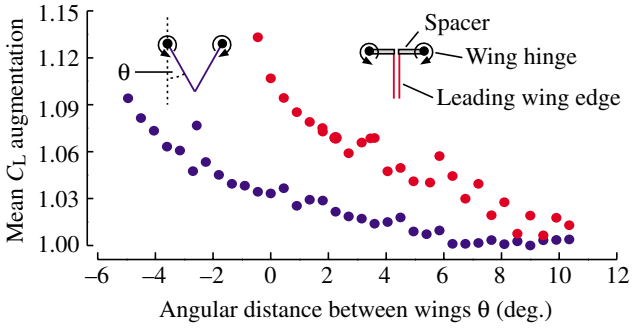

Fig. 2. Enhancement of mean lift coefficient for different near-clap conditions scaled to the performance of a single flapping robotic wing. The magnitude of lift coefficient C_L augmentation is 1.0 at large separation angles where the lift coefficients for one-wing and two-wing flapping are equal. Due both to the separation between the two wing hinges (gear box of the robot) and the rigidity of the model wing, the wings are closest at their tips (blue). Adding spacers at the wing hinge (red) reduces the dead space within the gap formed by the two wings during the clap. This experimental modification results in a higher aerodynamic performance at minimum angular distance between the two wings.

Time course of force enhancements

The force vectors in Fig. 1A,C suggest that the increase in total force during fling results primarily from a sharp peak at the beginning of the downstroke. However, a closer inspection of the time traces reveals that the clap-and-fling influences force generation throughout the entire stroke. Fig. 3 shows the changes in total force measured normal to the wing surface (Fig. 3A), lift (Fig. 3B), and drag (Fig. 3C) produced by a single wing (red) and a wing in the presence of its image pair for a single stroke cycle (blue). To evaluate the influence of the image wing, we calculated the difference between the instantaneous total normal force (black), lift (red) and drag (blue) under the two conditions (Fig. 4). The influence of the

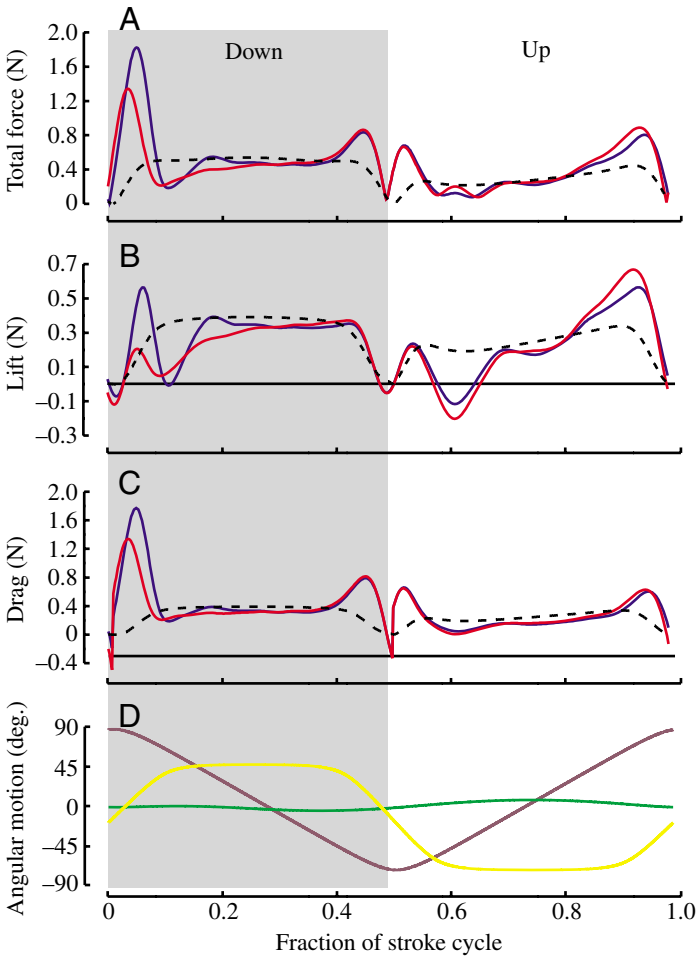

Fig. 3. Time traces of aerodynamic force production of the robotic wing throughout the stroke cycle when flapping a single wing (red) and when simultaneously flapping an imaged wing (blue) in close distance to elicit the clap-and-fling maneuver. (A) Total force production, (B) lift force that is equal to the force component in the vertical and (C) drag that is equal to force parallel to the horizontal. The broken lines in A–C indicate aerodynamic force production derived from a conventional analytical model for aerodynamics that solely depends on wing translational velocity and time averaged force coefficients (quasi-steady approach; for more details, see methods in Dickinson et al., 1999). (D) Translational wing motion (purple), the wing's angle of attack (yellow) and heaving motion (green) for a single stroke cycle.

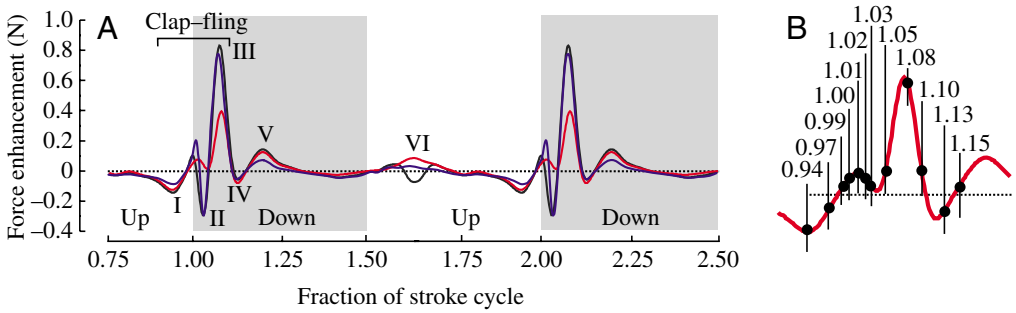

Fig. 4. Differences in aerodynamic force production between the performance of a single flapping wing (b) and when simultaneously flapping an imaged wing (a) at close distance to elicit a clap-and-fling wing beat. (A) Difference in total force production (a–b) normal to the wing surface due to wing–wake interaction are plotted in black; differences in lift production are shown in red and differences in drag are plotted in blue. The time traces demonstrate that dorsal wing interaction due to clap-and-fling may augment but also diminish force and lift production throughout the entire stroke cycle. Roman numbers (I–VI) label the main force peaks found in the data traces. (B) The small black dots during clap-and-fling indicate the times in fractions of the stroke cycle at which digital particle image velocimetry (DPIV) was performed. The stroke cycle starts and ends at $\hat{t}$=1.00 (dorsal wing excursion); however, due to the employed kinematic pattern the two wings clap (wings are held in parallel) about 1% or 50 ms after the beginning of the downstroke.

second wing is most obvious in six distinct portions of the wing stroke, labeled I–VI (Fig. 4). The augmentation of force due to image wing during the fling is clearly visible as a sharp peak (peak III). In contrast, the other features of the difference trace plotted in Fig. 4 were more subtle. Immediately prior to clap, there is a small attenuation of normal force and lift (negative peak I). At the earliest stages following the onset of fling, there is a small dip in the force (manifested mostly as drag, due to the high angle of attack of the wing; negative peak II). The sharp force augmentation during the fling (positive peak III) rapidly decays to a point at which force is slightly attenuated by the image wing (negative peak IV). Following this small attenuation, there is a second augmentation near mid downstroke (positive peak V). Finally, there is a small increase in lift during the upstroke, at which point the wings are far apart (positive peak VI).

To evaluate the relative contribution of each lift peak in Fig. 4 with respect to total lift enhancement, we measured the area under each peak. The required width of each peak was defined as the time between two successive zero crossings of the lift enhancement trace that enclose the peak. The combined effect of the fling (positive peaks III and V and negative peak IV) is an increase in mean lift and total force relative to the one-wing case of 9.6% and 9.2%, respectively, whereas the effect of the clap (negative peak I) was to decrease lift and total force by 4.3% and 2.5%, respectively. Thus, the net effect of the clap-and-fling is only 5.3% for lift and 6.7% for total force. In addition to these effects at the dorsal stroke reversal, however, we also found, quite unexpectedly, a change in force during the early upstroke (peak VI, Fig. 4). As also evident from the orientation of the force vectors in Fig. 1B,D, the total force production decreases whereas lift increases. Although the alteration in lift due to peak VI appears small, it amounts to an enhancement of 4.1%, and almost completely counterbalances the loss in lift production at the end of the upstroke preceding the clap (negative peak I, Fig. 4).

Velocity fields and leading edge vorticity

To investigate the aerodynamic mechanisms underlying the force and lift enhancements during the fling and the force attenuation during the clap phase, we conducted 2-D DPIV. We performed these measurements in five different sections perpendicular to the wing axes at 12 different times during dorsal stroke reversal (Figs 4B and 5) and in a section at the center of wing area. The chordwise flow at the center of wing area at approximately 65% wing length is shown in Fig. 5. In agreement with previous studies (Birch and Dickinson, 2001), we chose to quantify the flow velocity by averaging the values in a small region of the DPIV images close at the trailing edge of each wing, at a section of the wing at 65% wing length (grey areas, Fig. 6A) from $\hat{t}$=0.97 to 1.08 (Fig. 5C–J,O–V). Due to the arbitrary choice of the area under investigation and the vorticity distribution involved, the results and data shown in Fig. 6 must be interpreted with some caution (see next paragraph for the limits of DPIV analysis). Despite these potential errors, it is possible to compare the velocity fields at the trailing edge of one wing *vs* two wings because the investigation area is identical in both cases. The quantitative analysis shows that the average magnitude of the fluid velocity field in an investigation

Fig. 5. Sequence of wake structure during dorsal clap-and-fling maneuver when flapping one wing (upper rows, A–L) and flapping two wings (lower rows, M–X) generated by 2-D digital particle image velocimetry. The time values for each panel correspond to the time section before (negative values) or after (positive values) the clap occurs. Values in the images are fractions of the stroke cycle $\hat{t}$ (0–1). (A,M) –350 ms ($\hat{t}$=0.94); (B,N) –200 ms ($\hat{t}$=0.97); (C,O) –50 ms ($\hat{t}$=0.99); (D,P) 0 ms ($\hat{t}$=1.00); (E,Q) +50 ms ($\hat{t}$=1.01); (F,R) +100 ms ($\hat{t}$=1.02); (G,S) +150 ms ($\hat{t}$=1.03); (H,T) +300 ms ($\hat{t}$=1.05); (I,U) +450 ms ($\hat{t}$=1.08); (J,V) +600 ms ($\hat{t}$=1.10); (K,W) +750 ms ($\hat{t}$=1.13); (L,X) +900 ms ($\hat{t}$=1.15). The wing section at the center of wing area is indicated by a white line. The leading edge of the dorsal wing surface is marked by a white half circle. Fluid flow velocities are plotted in color code and arrows correspond to velocity vector at each point in the fluid; longer arrows signify larger velocities.

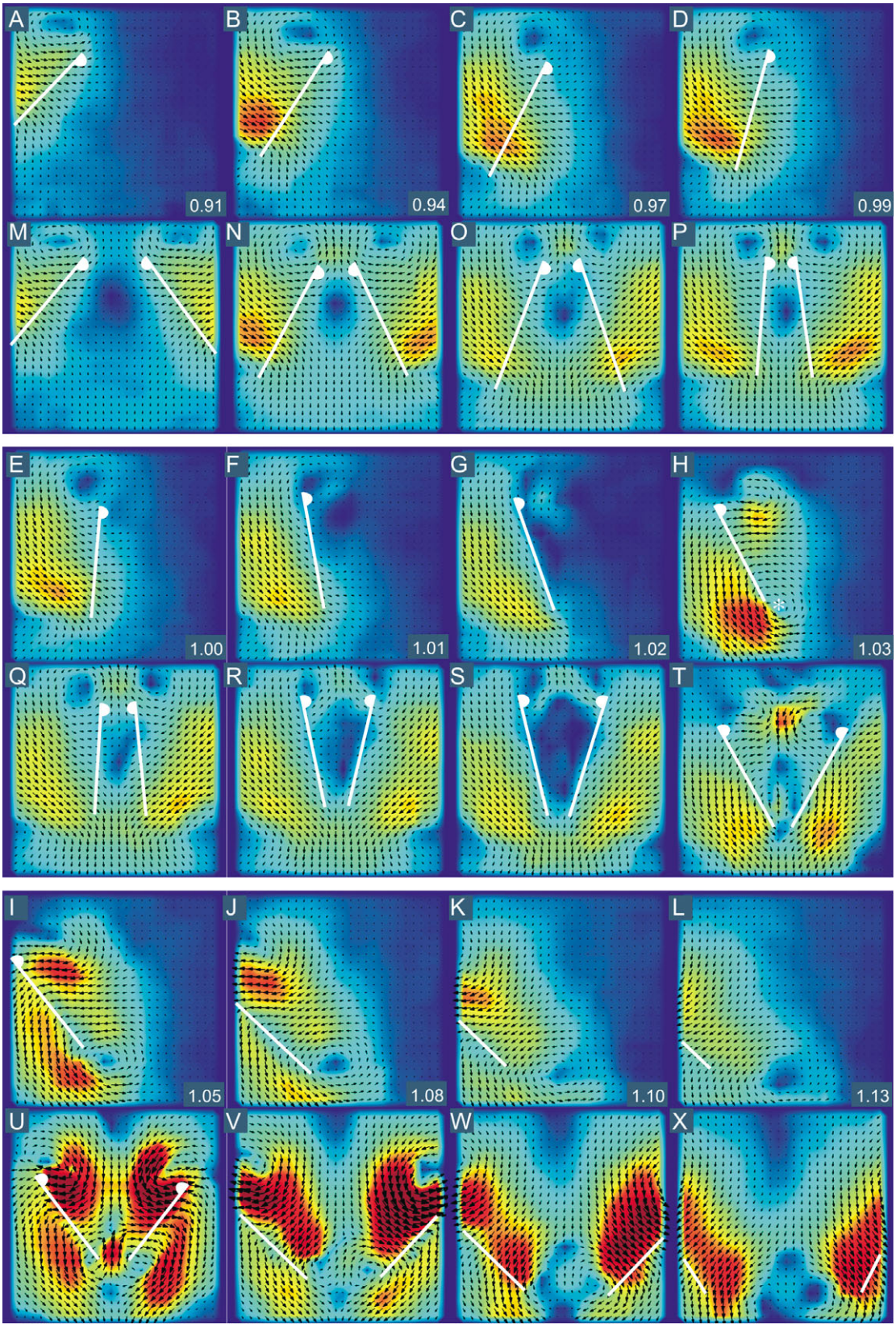

Fig. 5. See previous page for legend.

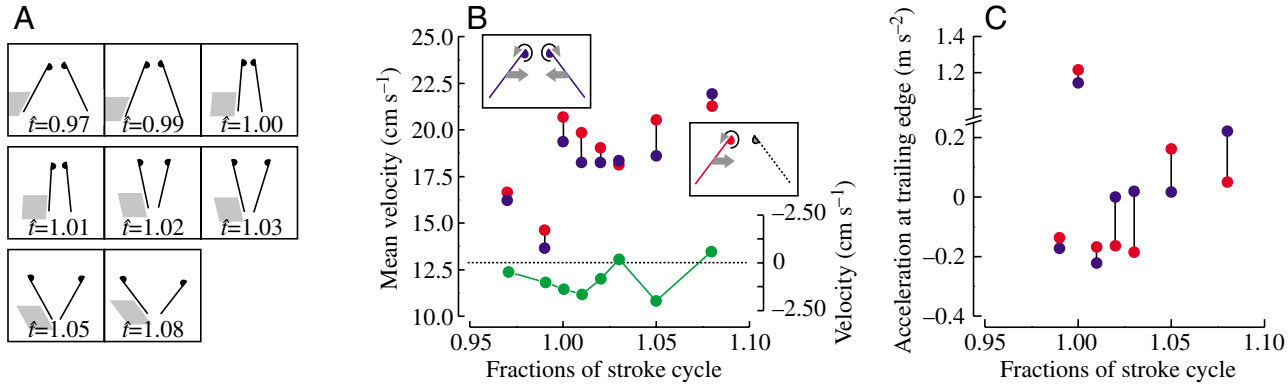

Fig. 6. Estimation of fluid velocity and acceleration in a local area near the trailing wing edge during one-wing and two-wing flapping conditions. (A) Grey areas indicate the regions of interest at eight different times during dorsal stroke reversal. (B) Mean flow velocity and (C) acceleration in the fluid when flapping one (red, lower pictogram) and two wings (image wing, blue, upper pictogram). Green data in B (right scale) show the difference in flow velocity between both flapping conditions. Acceleration fields were calculated from the difference of two subsequent DPIV images taken at 65% wing length (center of wing area). Stroke kinematics is the same as in Fig. 1.

area ventral to the trailing edge in the one-wing case is slightly higher (18.8±3.9 cm s^{-1}, mean ± S.D., N=8 different times from $\hat{t}$=0.97 to $\hat{t}$=1.08) than the fluid velocities in the same region in the two-wing case (18.0±3.6 cm s^{-1}, Fig. 6B). Neither the mean velocity estimates nor mean temporal change in fluid velocity (mean acceleration for one wing=0.11±0.51 m s^{-2}, two wings=0.14±0.46 m s^{-2}, N=7 different times from $\hat{t}$=0.97 to $\hat{t}$=1.08) in the investigation area differ significantly between the one-wing *vs* two-wing flapping condition (*t*-test on means, P>0.05).

Previous analyses of the clap-and-fling maneuver predicted that the leading edge vortices are stronger, due to an influx of fluid as the wings fling apart at the onset of the downstroke. To quantify the circulation of these vortices, we calculated the spatial distribution of vorticity in all five layers. The vorticity distributions of the fluid layer at the wing's center of area (layer at approximately 65% wing length) are shown as a time sequence during dorsal stroke reversal (Fig. 7). The LEVs formed in the two-wing case appear stronger than those generated by an isolated wing (Fig. 7F–J,R–V). To derive a quantitative description of leading edge vorticity during clap-and-fling we estimated the magnitude of leading edge vorticity in regions enclosing the LEV. Because of the changing flow pattern and growth of the LEV, we had to vary the size and shape of these regions, as indicated by the white areas in Fig. 7. For example, because of the stroke reversal, the region of interest is on the ventral side of the wing during the upstroke and on the dorsal side during the downstroke. Moreover, the proximity of the two wings during stroke reversal forced us to define much smaller regions of interest during the initial phase of the fling compared to regions at the end of the downstroke (clap phase) and late fling wing motion. The changing region size implies large uncertainties for estimating leading edge vorticity because the total circulation of a region will depend critically on region size, and most DPIV studies address this by increasing the region size until the circulation estimates asymptotes. Alternatively, we also estimated LEV circulation by a line integral using the automatic streamtrace tracking tool in Insight (TSI) to get the vortex contour and thus to separate the vortex from the surrounding fluid. However, because of the complex vortex shape and proximity of vortices with opposite spins, in many cases the streamlines did not enclose the vortex core. For this reason we decided to simplify our analysis and use the investigation areas as shown in Fig. 7. A detailed and excellent discussion about the limits of DPIV analysis for deriving forces from fluid velocities and their derivatives is given by Noca et al. (1999). More recently, Spedding (2003) suggested a model in which drag coefficients of rectangular wings can be calculated from wake momentum measured in birds flying in a wind tunnel (Rosen et al., 2004; Spedding et al., 2003a,b).

Besides the problems in estimating forces from flow acceleration, the temporal change in moment of vorticity is also required to derive a complete description of the fluid flow, which is not considered in the present study. All DPIV parameters mentioned above are eventually constrained by the two-dimensionality of the image planes that, in case of vorticity, only allows estimations of the curl of fluid particles in one out of three dimensions, thus ignoring any three-dimensional transport of vorticity. Moreover, the projection of three-dimensional components onto a two-dimensional plane (2-D-DPIV) underestimates total magnitude of vorticity except in the case in which all vortex lines are normal to the observation plane. In sum, given the various constraints on our

Fig. 7. Sequence of vorticity distribution in the wake at 65% wing length during single wing flapping (upper rows, A–L) and flapping two wings (M–X) using clap-and-fling wing beat pattern in the robotic wing. White boxes in the images show the region in which leading edge vorticity has been measured within the fluid. Vorticity is plotted according to the pseudo color code and arrows indicate the magnitude of fluid velocity; longer arrows signifying larger velocities. See Fig. 5 for temporal spacing between the images and more details. Values in the images are fractions of the stroke cycle $\hat{t}$ (0–1).

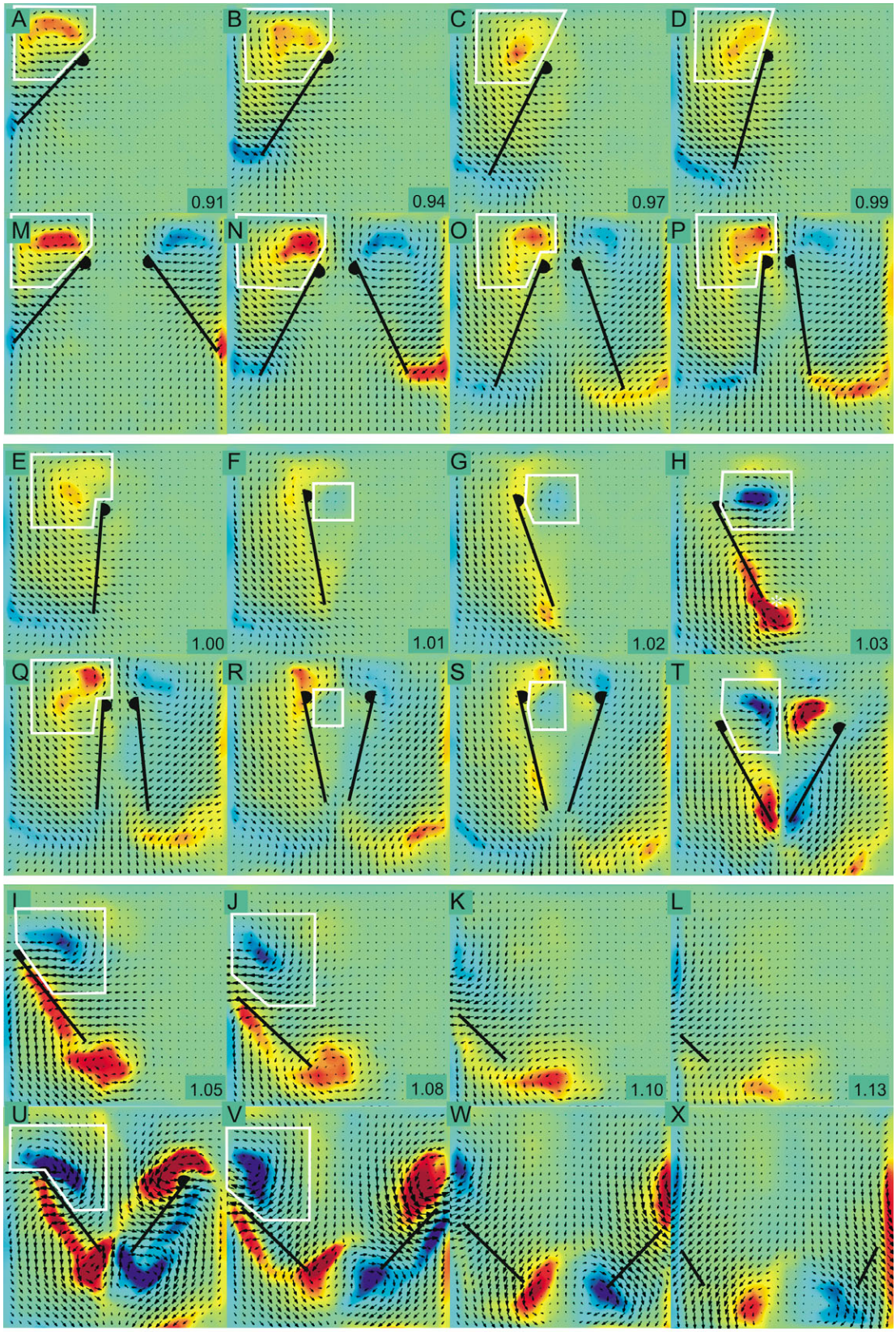

Fig. 7. See previous page for legend.

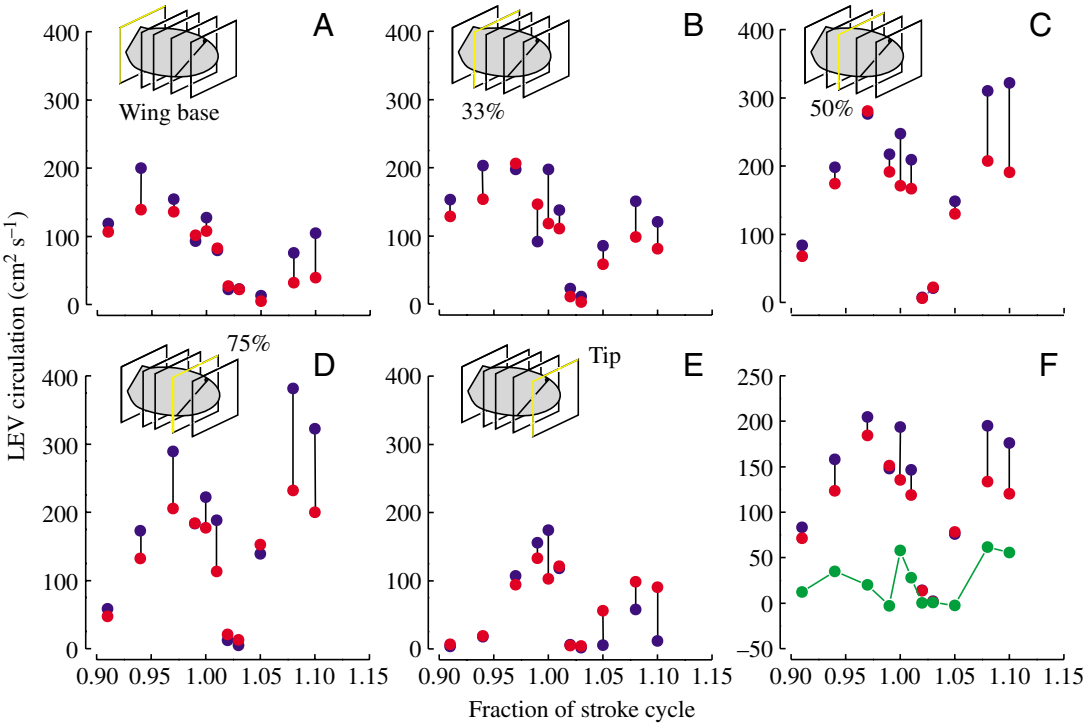

Fig. 8. Estimates of circulation of leading edge vortex (LEV) during dorsal stroke reversal in the robot while flapping its wings as shown in Fig. 1A–D. (A–E) LEV circulation measured at five different distances from the wing base. Pictograms illustrate wing shape and the yellow layer in each pictogram indicates the DPIV layer that was used for the analysis. LEV circulation for a single wing flapping is shown in red; when flapping two wings, in blue. (F) LEV circulation throughout the clap-and-fling maneuver and averaged over all five DPIV layers (cf. Materials and methods). Green data show the difference between both flapping conditions and demonstrate how LEV vorticity increases due to wing–wake interference during clap-and-fling.

circulation estimation during the fling phase, the data shown in Figs 8 and 9 are not intended to exactly match the instantaneous forces produced by the moving wing. However, even if the changes of circulation over time are suspect, the difference in leading edge vorticity between the one-wing and two-wing cases at one specific flapping phase can be assessed more reliably, because in this case the two DPIV integration areas have similar size and shape. To quantify flow conditions in the opening gap during fling from DPIV, we provide two estimates: average values of vorticity passing through the investigation area (LEV circulation), and the local peak values of vorticity within the LEV core.

Average circulation of the LEV for each sequence of the clap-and-fling maneuver is plotted for the fluid layer close to the wing base (Fig. 8A), at one-third distance to the wing base (33%*R*, Fig. 8B), at 50%*R* (Fig. 8C), at three-quarter distance (75%*R*, Fig. 8D) and close to the wing tip (Fig. 8E). The averaged values for all five layers are shown in Fig. 8F. The results show that circulation due to leading edge vorticity is slightly higher, by up to 57 cm^2 s^{-1}, at the end of the upstroke in the two-wing case (Fig. 8F). However, this result is not intuitive with respect to the force and lift measurements during wing motion preceding the clap and thus cannot explain why total force is attenuated at this time in the stroke cycle (peak

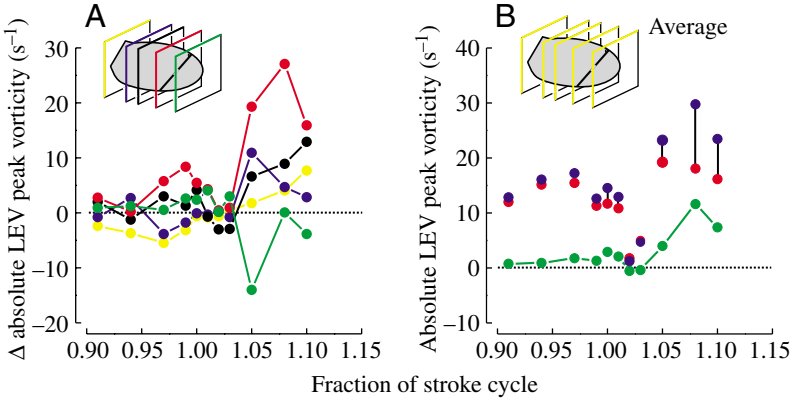

Fig. 9. Peak vorticity of LEV core and difference in peak vorticity between single-wing and two-wing flapping conditions. Peak vorticity was measured within the investigation areas shown in Fig. 7. (A) Difference (a–b) in peak vorticity between the one- (b) and two-wing (a) flapping conditions at five different DPIV layers, as indicated by the pictograms. (B) Averaged values of all five DPIV layers. Absolute LEV peak vorticity while flapping one wing is plotted in red; peak vorticity while flapping two wings is shown in blue. Vorticity difference (a–b) in B is shown in green.

I, Fig. 4A). During the clap phase, LEV circulation collapses to zero. Subsequently, LEV circulation builds up strongly during the fling phase in the two-wing case, reaching a magnitude of approximately 196 $cm^2\ s^{-1}$ at $\hat{t}$=1.08 fractions after the clap. The magnitude of LEV circulation at this stroke phase is similar to the maximum value of 207 $cm^2\ s^{-1}$ measured at the end of the upstroke ($\hat{t}$=0.97, Fig. 8F). In contrast, in the single-wing case, circulation of the LEV after clap reaches a maximum of 133 $cm^2\ s^{-1}$ at $\hat{t}$=1.08, which is 28% less than the value prior to the clap, corresponding to a difference of approximately 52 $cm^2\ s^{-1}$ (from 185 $cm^2\ s^{-1}$ to 133 $cm^2\ s^{-1}$; Fig. 8F). The maximum difference in LEV circulation during the fling phase between the one-wing and two-wing cases was 63.0 $cm^2\ s^{-1}$, or 32% of the two-wing case, measured at $\hat{t}$=1.08.

Quite similar to the differences in LEV circulation between one- and two-wing flapping, absolute peak vorticity of LEV increases during the fling phase when flapping the image wing (Fig. 9). We found that LEV peak vorticity, averaged over all five spanwise DPIV layers, increases up to approximately 12 s^{-1} or 50% when flapping both wings, compared to its value for a single wing (Fig. 9B). The maximum increase in LEV peak vorticity was obtained at $\hat{t}$=1.08 fractions after the clap and at approximately two-thirds wing length: at 65%*R* (center of wing area; peak vorticity of one wing=25.6 s^{-1}; two wings=50.7 s^{-1}; difference=25.1 s^{-1}) and 75%*R* (peak vorticity of one wing=23.2 s^{-1}; two wings=50.2 s^{-1}; difference= 27.0 s^{-1}). These results are consistent with the delayed increase in LEV circulation, as outlined in the previous paragraph. Although neither the circulation estimates nor the peak vorticity values of LEV are sufficient to derive aerodynamic forces from the flow measurements using analytical models, the results show qualitatively the enormous influence of the image wing on LEV strength and circulation during fling motion.

Fling coefficients

The flow fields in Fig. 7 were also used to test the theoretical predictions of the strength of the LEV during the fling maneuver. We calculated the rotational coefficient $\boldsymbol{g}(\theta)$ from DPIV using the data shown in Fig. 8, which depends on the angle of wedge between the wings (total angular separation) prior to translation. There is a chance that the high force values during clap-and-fling might have slightly changed the programmed kinematics of the wings because of some play between the gears of the robotic model. For this reason, we directly measured the geometrical angle of attack of the rotating wings from their location in the DPIV images. The mean angular velocity during the fling, based on these measurements, was 74.1 deg. s^{-1} (Fig. 10A). Fig. 10B shows the function $\boldsymbol{g}(\theta)$ according to Eq. 2, using the values of LEV circulation derived from the measured flow data shown in Fig. 8 for each of four different chordwise sections (33%, 50%, 75% and 100%*R*). The chord length for these sections was 0.094, 0.094, 0.11 and 0.11 m, respectively. The data show that in the 50% section, $\boldsymbol{g}(\theta)$ increases with total gap angle up to a value of 3.5 at an opening angle of approximately 73°, then decreases slightly as the gap approaches 90°. This result is consistent with prior flow measurements from a single wing moving at similar Reynolds number, which indicates that the chordwise circulation is maximum close to a spanwise location of 65%*R* (Birch and Dickinson, 2001; Ramamurti and Sandberg, 2001). At gap openings below 30°, $\boldsymbol{g}(\theta)$ remains less than 0.3 in all sections. The increase of $\boldsymbol{g}(\theta)$ with increasing gap angle highlights the difference between the 3-D experimental results obtained in a real fluid and Lighthill (1973)'s 2-D inviscid-flow model, which reaches maximum $\boldsymbol{g}(\theta)$ at the beginning of the fling phase (blue line, Fig. 10C). The 2-D inviscid model provides a reasonable match with the 3-D experimental data at gap angles above 73° (Fig. 10C).

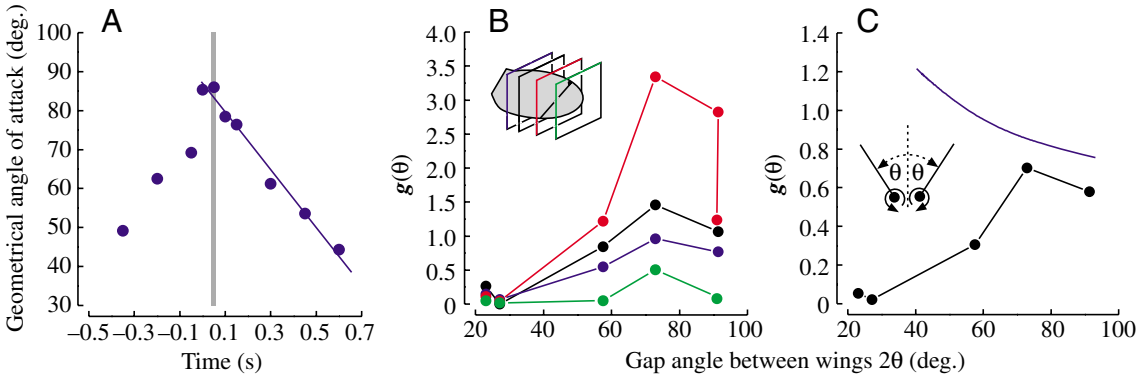

Fig. 10. (A) Geometrical angle of attack of the robotic wing as measured from the DPIV images. The time values correspond to the time section before (negative values) or after (positive values) the clap occurs (gray line). The small jitter in angular wing position might be due to mechanical play within the robotic wing hinge. Rate of change in geometrical angle of attack during fling phase amounts to approximately 74 deg. s^{-1} (linear regression fit, y=87.1–74.1x). (B) Rotational coefficient for LEV circulation during fling using Lighthill (1973)'s analytical model for inviscid flow conditions. The function $\boldsymbol{g}(\theta)$ is equal to LEV circulation normalized to angular speed of wing rotation and wing chord. Color coding of the data points corresponds to the five different layers used for the DPIV measurements (see pictogram). (C) Mean values for the rotational coefficient $\boldsymbol{g}(\theta)$ (black), calculated from the five DPIV layers as shown in B. Analytical function modeling inviscid flow conditions during the clap-and-fling kinematics of the parasitic wasp *Encarsia formosa* is plotted in blue (replotted from Lighthill, 1973). See Materials and methods for more details.

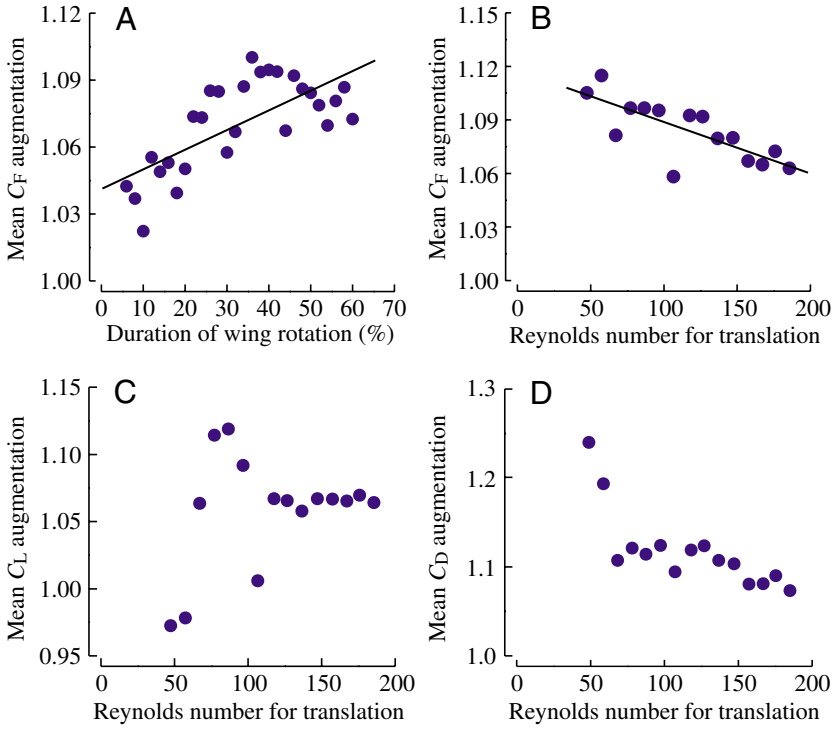

Fig. 11. Augmentation of mean force coefficient during clap-and-fling wing beat plotted as a function of duration of wing rotation within the stroke cycle (A) and Reynolds number based on wing tip speed velocity (B). Augmentation of mean lift and drag coefficient due to clap-and-fling, scaled to the performance a single flapping wing is shown in (C) and (D), respectively. Angular distance between the wings during clap was –4.95°. For these experiments we modified a conventional stroke pattern (stroke amplitude=160°, cycling frequency=0.16 Hz, geometrical angle of attack at mid stroke=50°, up/down ratio=0.5 and approximately symmetrical timing of wing rotation at which 50% of the rotational phase occurs before and 50% after the clap) by systemically varying the onset of wing rotation at the end of each half stroke (in A) and stroke frequency (in B–D).

Dependencies of clap-and-fling force augmentation

To investigate the dependence of clap-and-fling force augmentation on subtle or gross changes in stroke kinematics and local flow conditions, we systemically varied wing motion and Reynolds number using a generic stroke pattern (cf. Materials and methods). Fig. 11A shows that augmentation of the mean force coefficient increases approximately threefold, from about 3% to 9%, with increasing duration of dorsal wing rotation (linear regression, $y=1.04+8.78\times10^{-4}x$, $r^2=0.49$, $N=28$, $P<0.001$). However, although the linear regression is significant, the data show a decrease in lift augmentation for flip durations greater than 40% of the stroke durations suggesting that the contribution of clap-and-fling circulation to total force coefficient peaks at intermediate rotational velocities. By varying stroke frequency from 48.8 to 191 mHz, we could change the Reynolds number from approximately 47 to 186. The results indicate that even small changes in Reynolds number produce a significant effect on the mean force coefficient (Fig. 11B). With increasing Reynolds number, augmentation of the mean force coefficient decreases significantly from approximately 112 to 106% of the one wing value (linear regression, $y=1.12–2.87\times10^{-4}x$, $r^2=0.58$, $N=15$, $P<0.001$). This increase in the effectiveness of the clap-and-fling with decreasing Reynolds number is consistent with a recent 2-D simulation based on the immersed-boundary layer method of Miller and Peskin (2004). Most of this effect, however, appears to be due to drag because Fig. 11C shows that the augmentation of the lift coefficient tends to decrease with decreasing Reynolds number (linear regression, $y=1.02+3.02\times10^{-4}x$, $r^2=0.32$, $N=15$, $P=0.25$).

Discussion

The results of this study confirm previous research on the clap-and-fling mechanism and show that dorsal wing–wing interaction modestly enhances total normal flight force and lift production among insects flying at an intermediate Reynolds number. For wing kinematics modeled on tethered flying fruit fly *Drosophila melanogaster*, the magnitude and orientation of the mean force vector produced by wings during clap-and-fling generates a lift increase of 8.2% (mean lift: single wing=0.222 N; two wings=0.243 N). This enhancement occurs when the two wings are still in close proximity and the angular separation between them is less than about 10°, but vanishes at greater angular separations. The data further suggest that clap-and-fling enhancement does not require the wings to physically touch, so that even near-clap conditions can augment force. In contrast to earlier studies, we found that force augmentation during the fling phase is partially offset by a modest attenuation during the clap phase. The clap-and-fling also exerts a more indirect effect on forces through gross changes in far field flow and contributes to lift enhancement at the beginning of the upstroke when the wings are separated by approximately 90° – far exceeding the 10° separation required for force enhancement *via* the fling. As described in previous studies, a major source of force enhancement during the fling phase results from an influx of fluid into the opening cleft, which increases the strength of the leading edge vortex (LEV). However, in comparison to inviscid analytical models, the development of the LEV bubble is delayed in the real fluid although experimental data and theoretical results match more closely as translation continues (Figs 8 and 10). Moreover, by varying various aspects of the stroke kinematics the data show

that the relative contribution of clap-and-fling to normal force and lift production depends on several factors such as rotational duration during stroke reversal and Reynolds number.

Previous models

Most analyses of Weis-Fogh's clap-and-fling mechanism have largely focused on the fling phase and several studies clearly show that wing–wing interaction produces higher lift at the onset of downstroke. However, given the different experimental conditions and various assumptions of the analytical and experimental models (viscous *vs.* inviscid conditions and two- *vs* three-dimensional models), any comparison of our conceptual model with the idealized initial models by Weis-Fogh (1973), Lighthill (1973) and others should be done with care. In particular, axial flow from wing base to tip during three-dimensional wing translation may alter LEV shape and stability (Ellington et al., 1996; Usherwood and Ellington, 2002). Weis-Fogh's and Lighthill's original framework of the clap-and-fling was primarily two-dimensional with trailing wing edges completely connected. Because of this assumption neither author considered trailing edge vorticity in their studies on the clap-and-fling (see *peel*, below). The initial description of Weis-Fogh's and Lighthill's leading-edge separation bubble was later replaced by Edwards and Chen (1982), who introduced the concept of leading edge vorticity. In his two-dimensional analytical model of the clap-and-fling, Lighthill (1973) assumed an inviscid fluid. For this reason, circulation around a single wing is infinite at the initial fling motion because a calculation without vortex separation does not permit the accumulation of vorticity in the fluid. At small gap angles, the function $\boldsymbol{g}(\theta)$ in Fig. 10C (blue) thus starts at infinity. Moreover, Lighthill pointed out the modifications of clap-and-fling due to viscous effects including vortex shedding, but greatly underestimated the magnitude of the accumulation of circulation in the separation vortex. Maxworthy (1979) and Spedding and Maxworthy (1986) demonstrated this later for a two-dimensional system. Moreover, Maxworthy also conducted three-dimensional experiments at two vastly different Reynolds numbers of 32 and 13 000, and experimentally compared the dynamics of circulation produced in the opening wing cleft at different relative fluid viscosities. Bennett's experiments (Bennett, 1977) on the clap-and-fling at Reynolds number of 83 000 are slightly different because he used only one model wing with a vertical wall that mirrors the effect of the second moving airfoil. This assumption works well for the inviscid case at high Reynolds numbers because the wall gives an exact plane of symmetry. For the viscous case at moderate and low Reynolds numbers, however, the development of unsteady viscous boundary layers over the vertical plane most likely destroys three-dimensional vortex structures that potentially alter force production. Bennett reported that the model wing starting impulsively with fling motion generates 15% more lift in the presence of the vertical wall as compared to the control single wing. Using spacers to minimize the distance between our two model wings, we obtained a similar enhancement of about 13% at a moderate Reynolds number of 134 and three-dimensional flapping conditions (Fig. 2), although Bennett (1977) explicitly predicted that the effect of clap-and-fling would be negligible for small insects. Even more important, in contrast to our fruit fly model, which performs a full cycle motion involving both clap-and-fling and a ventral reversal, the model wing employed in all previous experiments (Bennett, 1977; Maxworthy, 1979; Spedding and Maxworthy, 1986) did not simulate the fling-preceding clap and thus ignored its deleterious effects.

Wake history and force attenuation during clap phase

The results reported here measured the time course of force variation between the two-wing *vs* one-wing case, and also examined the influence of the wake history of previous strokes on the time course of force production by clap-and-fling. These experiments also revealed that the force generated at the end of the upstroke is slightly attenuated in the presence of an image wing (negative peak I, Fig. 4). It is worth noting that the absence of vertical body motion in our experiments matches recent findings on vertical body oscillations during free flight hovering in *Drosophila* using high speed video analysis (Fry et al., 2003). As the wings start the clap, the presence of an image wing significantly diminishes the ability of each wing to accelerate fluid and thus generate aerodynamic forces. Alternatively stated, the presence of an image wing creates a circulation of opposite sense very close to the wing, thus diminishing its ability to build up circulation. This situation is analogous to the interaction between the starting and bound vortex of an impulsively started wing predicted by Wagner (1925). If correct, this hypothesis predicts that due to decreased circulation, less trailing edge vorticity is shed by the wing in the two-wing case than in the one-wing case. Evidence for this hypothesis is provided by a comparison of the peak trailing edge vorticity as it leaves the wing in Fig. 7B–D,N–P (absolute peak vorticity in grey area of Fig. 6A, time slice $\hat{t}$=0.97: one wing=1.13 s^{-1}; two wings= 0.90 s^{-1}). The DPIV images suggest that trailing edge vorticity, and thus the bound circulation at $\hat{t}$<0.99, are considerably stronger for the single-wing case than for the two-wing case at an identical time interval. As the wing rotates in preparation for clap, and the stopping vortex is shed, the leading edge vorticity builds up and total force begins to rise due an increase in bound circulation (Fig. 7B–E,N–Q). Although in large part this build-up results from rotational circulation, the presence of an image wing enhances the leading edge vorticity generated per unit time, suggesting some modification of circulation during clap.

At the instant of clap, there is a slightly higher force in the two-wing case than the single-wing case (Fig. 4B, time slice $\hat{t}$=1.0). Ellington (1984b) and also Götz (1987) suggested that a modest increase is likely due to a jet of fluid squeezed out of the closing gap between the trailing edge during the later portion of the clap phase. Brodsky (1991), using smoke streams, also suggested a jet mechanism during wing pronation in the peacock butterfly *Inachis*. As evident from Fig. 5O,P,

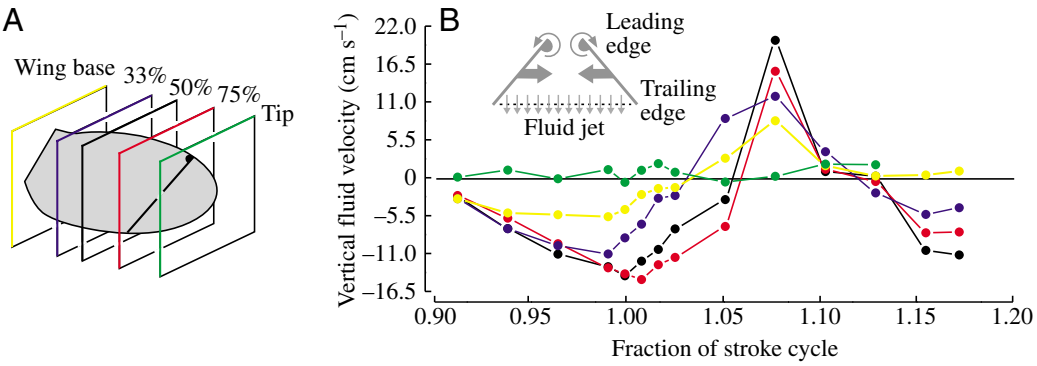

Fig. 12. Fluid jet velocities associated with fluid motion out of the gap during wing motion preceding the clap, and fluid motion into the gap during fling phase. (A) Pictogram illustrating wing shape and the layers (as a % of *R*) used for digital particle image velocimetry (DPIV). (B) Temporal change of local vertical fluid velocities averaged along a line between the two trailing wing edges during clap-and-fling wing motion. Data were derived from DPIV images and show fluid velocities at five different distances to the wing base. A negative value means that the fluid is moving downwards in a vertical direction (downward jet). A positive value means that fluid is sucked around the trailing wing edges into the 'v'-shaped cleft from below. Color coding as in A.

there is indeed a small downward jet of fluid, which may account for this modest increase in force in the final phase of clap. In Fig. 12 we estimated the velocity of this fluid jet during two wing flapping conditions. The data suggest that at the end of clap motion (time slice $\hat{t}$=1.0), the velocity of the fluid leaving the gap reaches up to 15 cm s^{-1}, corresponding to approximately 50% of the maximum velocity we measured during the entire sequence of clap-and-fling wing motion. For comparison, a recently published 2-D simulation of the clap-and-fling at Reynolds number of 17 by Sun and Yu (2003) suggests that the wings generate consistently higher forces for the two-wing case than the one-wing case, rather than an initial decrement (clap attenuation, peak I) followed by a modest rise as seen in the experiments performed here. At present, it is not clear if this discrepancy results from the differences in Reynolds number or the two-dimensionality of the simulations in Sun and Yu (2003).

Force enhancement during fling

The time traces following the fling reveal a complex pattern of force augmentation and attenuation. In particular, lift decreases below the single wing case approximately 0.1 fractions of the stroke cycle after the fling (negative peak IV, Fig. 4) followed by a sharp increment (positive peak V, Fig. 4). This fluctuation arises from a delayed rise in peak forces in the two-wing case. In the initial part of the fling, the one-wing case reaches a peak slightly earlier than in the two-wing case. For a short duration after the fling, the total force for both the two-wing and one-wing cases rises at roughly the same rate, but peaks earlier in the single-wing case than the two-wing case. For the fling, this peak continues to rise to a higher value even as the single wing force begins to fall, resulting in the sharp fling-related peak centered around $\hat{t}$=1.08 (Fig. 4B). Following these early events, the single wing force falls to a slightly higher value than the fling case, resulting in a modest negative peak IV, between peaks III and V. Whereas the net forces slowly reach steady values in both cases, in the case of fling they attain a steady value earlier, leading to the second peak (peak V).

The corresponding events are visualized using DPIV in Figs 5 and 7. Although the flows were imaged at five different sections along the wing, in addition, we chose a section through the center of the wing area most representative of the total force on the wing (65%*R*). As in case of the clap, these images reveal substantial differences between the present and previous studies on this topic. As the wings fling apart, there is a rapid build-up of leading edge vorticity (Fig. 7E–L,Q–X). In this initial stage (Fig. 7F–H,R–T), two prominent effects appear to influence the circulation around each wing. First, the presence of counter-circulation on the image wing appears to inhibit the initial rise in circulation (Fig. 7F–G,R–T). Second, as the wings fling apart further, the influx of fluid from above into the low pressure region between the wings induces a strong leading edge vorticity, causing a sharp rise in force. The possible reasons for the inhibition of the early growth of LEV might be the following: first, unlike in Weis-Fogh's original model that was derived from the wing kinematics of the small wasp *Encarsia formosa*, wing separation in our robotic model allowed trailing edge vortices to form at the early fling phase (Fig. 7T). The presence of trailing edge vorticity may inhibit the development of leading edge vorticity because fluid is accelerated in the opening cleft from below, potentially interacting with the development of LEV and creating an upward momentum.

Effects of wing–wing proximity

Some past studies on insect flight have described variations of clap-and-fling such as 'near clap-and-fling' (Ellington, 1984a; Ennos, 1989) and the clap-and-'peel' (Götz, 1987). The relative contributions of these various mechanisms to aerodynamic forces are functions of the proximity of the two wings as well as their independent patterns of motion. Our work addressed these effects in two ways. First, to estimate the effect of near-clap conditions, we varied the angular distance

θ between the wings at the start of the dorsal reversal from –4.95° to 10° (total angular separation= –9.9 to 20°, Figs 1 and 2). At a fixed distance between the wing hinges, the tips of the two wings nearly touch each other at θ=–4.95°, whereas at 0° the wings are exactly parallel at stroke reversal, but their tips are at a greater distance from each other. Under these conditions, the effects of wing–wing interactions are quite evident (Fig. 1). At a starting angle θ of approximately 10°, the difference in mean force between one and two wings is zero, suggesting that at these large spatial separations, the wings do not influence the development of circulation on each other. The total angular separation required for significant wing–wing interaction must vary with Reynolds number, which determines the degree to which the wings will develop their own starting vortex. However, from the results shown here, we can conclude that for insects flying in a Reynolds number range comparable to our *Drosophila*-based model, wing kinematics with total angular separation (2θ) of less than 20° at dorsal stroke reversal is sufficient to result in a significant wing–wing interaction.

Second, to examine the effects of the clap involving a close juxtaposition of the entire area of the wings, we attached spacers to the wings to allow them to interact more closely (Fig. 2). These modifications enhance lift modestly by an additional ~3.9% of the performance of a single wing, suggesting that a closer juxtaposition of the entire area might have potential benefits towards force generation. However, since the spacers also displaced the wing surface from the rotational axis of the robot's gear box, some of the enhancement might be due to the changes in the overall performance of the two wings. Because of the distance between the left and right wing hinge in both the robot and in insects, a close juxtaposition of the entire area of the wings can only be achieved when the wings bend at the wing root, which was shown by high-speed photographs in tethered flying *Drosophila* (Götz, 1987; Lehmann, 1994). Because the model wings used in these experiments are rigid, they only approximate a full clap by allowing a greater interaction between the area of the two wings and do not exactly replicate it. Thus it is likely that the elasticity of the wings allows the animal to increase the size of wing contact area during a full clap (time of stroke reversal) in order to enhance the efficacy of LEV induction during fling motion.

Upward momentum during fling and a new explanation for the peel

In contrast to the rectangular shape of model wings used in previous studies on the clap-and-fling (Bennett, 1977; Maxworthy, 1979; Spedding and Maxworthy, 1986; Sunada et al., 1993), most insect wings such as *Drosophila* are more or less oval in shape. As a result, the clap-and-fling motion in rectangular wings occurs with its trailing edges closely aligned, and the trailing edge region remains impervious to fluid throughout the entire motion of the fling. In contrast, the oval wings in our experiments were only close in a small region at the tip of the wing during fling, and fluid is admitted into the region between the wings from all directions. In other words: in oval wings, it is impossible to have full trailing wing contact (as assumed in Weis-Fogh's and Lighthill's original models) during fling unless the elasticity of the wings allows the wings to bend along their chords. This kinematic maneuver is termed *peel*, and has been described in many larger insects such as various species of butterflies, bush cricket, mantis and locust (Dalton, 1975; Cooter and Baker, 1977; Ellington, 1984a; Brackenbury, 1990, 1991a,b; Brodsky, 1991). The peel kinematics was originally suggested as a mechanism to accelerate the fluid into the cleft more smoothly (Weis-Fogh, 1973; Ellington, 1984b). In rigid oval wings, the opening between the trailing wing edges allows fluid to enter the cleft from the rear while lowering lift production due to the fluid's momentum (see direction of fluid vectors in Fig. 5U, the increase in vorticity in the rear cleft in Fig. 7U, and Fig. 12). The opening might also allow trailing edge vorticity to shed into the wake, similar to the shedding of the starting vortex in the single-flapping wing case (Fig. 7I–L,U–X). Thus the possible explanation of the sudden decrease in force/lift augmentation (peak IV, Fig. 4) is that the generation of strong trailing edge vorticity close to the wing's surface lowers the benefit of leading edge circulation. The *peel* offers a solution to this problem because it may function as a mechanism to prevent fluid being sucked into the cleft from the rear. This would increase lift production associated with the clap-and-fling maneuver by preventing the generation of an upward-directed momentum jet.

Wake capture force

In addition to far-field effects, clap-and-fling also influences near-field phenomena such as wing–wake interactions generated by flapping wings immediately following stroke reversal (Dickinson et al., 1999). The extraction of kinetic energy from the wake behind a freely flying insect has been demonstrated in a study of butterflies during take-off, in which smoke trails were used to visualize the flow around the moving wings (Srygley and Thomas, 2002). Because wing–wake interactions may depend on the distribution of vorticity shed at the start of each stroke, they may be weaker when less vorticity is shed at the end of the prior half stroke. This is similar to increasing the strength of the inter-vortex stream produced by trailing and leading edge vorticities (Fig. 13; Dickinson, 1994). As seen in Fig. 7B–D,N–P, it seems that there is a small decrease in the vorticity shed at the trailing edge as the wing approaches clap. Because this change potentially lessens the velocity of the inter-vortex stream (Fig. 5B–D,N–P), as indicated by the decrease in the difference of flow velocity between both experimental conditions (Fig. 6B), we expect a decrease in forces immediately following stroke reversal for the two-wing case as compared with the one-wing case. This hypothesis is borne out by the presence of negative peak II (Fig. 4A).

Extraction of kinetic energy from the wake during wake capture should result in a deceleration of fluid motion. Superficially, Fig. 6C shows a small difference in fluid

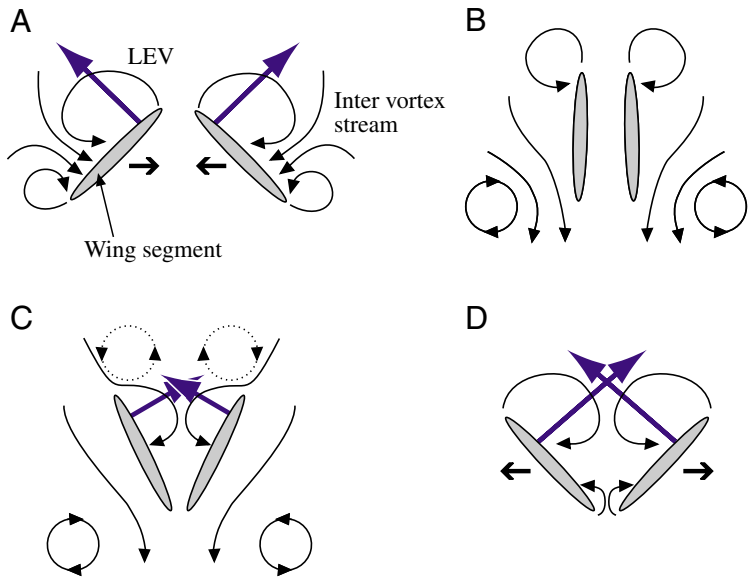

Fig. 13. Schematic reconstruction of vortex generation and shedding during the clap-and-fling maneuver using a generic *Drosophila* stroke kinematics. (A) Chordwise wing segments at the end of the upstroke, (B) during the clap phase of the two wings, (C) during the early fling phase and (D) the late fling right before the two wings separate for the downstroke. Leading and trailing edge vortices that are generated during the upstroke are shed into the wake at the end of each half stroke. The vortex system generates an inter-vortex stream towards the wing that is thought to enhance flight forces *via* momentum transfer. Due to near-clap conditions the low pressure region evolving between the wings during the fling pulls fluid around the leading and the trailing wing edges into the opening cleft.

acceleration between the one-wing and two-wing flapping cases after the clap, with a pronounced deceleration (negative acceleration values) of fluid in the single-wing case during the early fling phase. This deceleration in the single-wing case at $\hat{t}$=1.01–1.03 coincides with the relative decrease in augmentation of normal force (two-wing minus one-wing force) immediately after the clap (peak II, Fig. 4), suggesting that at this time, a single wing may extract more kinetic energy from the wake than in the two-wing case. However, the general problem in interpreting the possibility of modified wake capture force, particularly later in the stroke at $\hat{t}$=1.08 (time when peak III occurs, Fig. 4), is that wing separation angle 2θ already amounts to approximately 75° and the normalized LEV circulation $\boldsymbol{g}(\theta)$ has fully developed, close to the prediction of 2-D inviscid theory (Fig. 10C). The increase in fluid acceleration, for example, in the two-wing case at $\hat{t}$=1.08 (Fig. 6C) could thus be driven at least partly by LEV-induced downwash that might in turn override the effect of possible modifications in wake capture force.

Even so, if we assume that modification in wake capture force is responsible for the primary peak of force enhancement during clap-and-fling (peak III), then peak IV in the force trace should not be regarded as a decrease in LEV induced force/lift enhancement (Fig. 4), but rather a delay between the wake effect and a subsequent enhanced growth of the LEV. In this scenario, peak V would simply result from strong leading edge vorticity at large separation angle when the wing has reached its maximum translational velocity during the downstroke (Fig. 10B,C). It is worth noting, however, that peak V appears relatively late in the downstroke at $\hat{t}$=1.2, whereas fling circulation, as indicated by $\boldsymbol{g}(\theta)$, has fully developed by $\hat{t}$=1.08 (Fig. 10C). Since at $\hat{t}$=1.1 the wing's leading edge has moved out of the DPIV field of view, we were not able to quantify the entire time course of LEV development during the downstroke, and thus cannot offer a detailed explanation for the transient peak of force/lift enhancement (peak V, Fig. 4).

Vortex symmetry and Reynolds number effect

In the conventional view, the inhibitory effect of viscosity on fluid acceleration commonly predicts that lift forces produced during wing motion should decrease with decreasing Reynolds number. For example, the performance of a single *Drosophila* model wing flapping with a generic kinematic pattern decreases linearly with decreasing Reynolds number (*Re*= 30–200, 2-D in Dickinson and Götz, 1993; 3-D in Lehmann, 2002), which is consistent with recent CFD (computational fluid dynamics) predictions on the aerodynamics of wing flapping in small insects at low Reynolds numbers (Miller and Peskin, 2004; Wu and Sun, 2004). Miller and Peskin argue that mean lift, but not drag, produced by a single, isolated wing decreases with decreasing Reynolds number, due to the prolonged attachment of the trailing edge vortex, which they termed 'vortex symmetry'. This effect may be explained by noting that if the leading and trailing edge vortices move together there is no change in the moment of vorticity and thus no lift generated in the direction orthogonal to motion (Wu at al., 1991). This symmetry deteriorates at Reynolds numbers above approximately 32. At this point the trailing edge vortex sheds at the start of translation and the moment of vortices changes steadily throughout motion, resulting in lift. The same 2-D CFD model also suggests an increase in relative contribution of the clap-and-fling to lift as Reynolds number decreases (Miller and Peskin, 2005). This curious result, relative to the isolated wing case, results from the effect of Reynolds number on the interaction between the trailing edge vortices. At low Reynolds numbers the proximity of the trailing edges at the onset of translation inhibits the formation of trailing edge vorticity. Thus, at lower Reynolds number, the leading edge vortices are stronger and serve as each other's starting vortex to maintain Kelvin's Law. The data we estimated for total normal force enhancement due to the clap-and-fling in the *Drosophila* model wing show the same trend (Fig. 11B). At a Reynolds numbers of approximately 50, the force augmentation due to the fling is greater than at a Reynolds numbers of approximately 200. However, in contrast to the results of the 2-D simulations, we found no evidence that the lift produced during the fling increases with decreasing

Reynolds number (Fig. 11C). Such a discrepancy might arise from 3-D effects, or the fact that the separation between the trailing edge of the wings was greater in our experiments than in the 2-D simulations of Miller and Peskin (2005).

An alternative explanation for this effect is that the relative increase in viscous forces at low Reynolds number requires higher forces to pull the wings apart during fling motion and thus drag coefficient augmentation increases with decreasing Reynolds number (Fig. 11D). However, this explanation is not inconsistent with that which emphasizes the role of Reynolds number on the formation of the leading edge vortices; both phenomena are different manifestations of the influence of viscosity. It is important to emphasize that while viscosity can subtly enhance lift generated during the fling at low Reynolds number, it increases drag to an even greater degree. Thus, the lift-to-drag ratio becomes less favorable with decreasing Reynolds number (Fig. 1G), and the clap and fling cannot be viewed as a mechanism to improve this performance parameter. This is not necessarily inconsistent with the observations that tiny insects are more dependent on the flap and fling, assuming that they are limited by lift and not power.

Conclusions

The results of this study on the dorsal clap-and-fling mechanism in flapping wing motion of a 'hovering' robotic fruit fly wing has revealed an unknown complexity of flight force modifications throughout the entire stroke. The main differences between our findings and previous analytical and experimental studies are: first, the clap part of wing motion attenuates total force and lift and does not generate even larger lift force than the initial phase of the fling, as found in another 3-D model wing (Maxworthy, 1979). Second, potential modifications of wake capture and viscous forces fling might explain some of the changes in total force and lift production during clap-and-fling. And third, the clap-and-fling wing beat seems to distort wake structure throughout the stroke cycle, as indicated by the unexpected peak of lift enhancement at the beginning of the upstroke. In sum, knowledge of the fluid mechanical mechanisms and physical constraints underlying wing–wake interactions in flapping flight may broaden our understanding of how the different forms of wing kinematic patterns, including the clap-and-fling, have evolved through their long evolutionary history. Given the constraints upon circulation development and endurance during clap-and-fling in real fluids, it seems evident that although total lift enhancement is modest, the clap-and-fling is a useful mechanism by which insects can elevate force production. Considering the short time over which fling-induced flight forces act, the enhanced locomotor performance might favor steering control in some insects performing elaborate aerial maneuvers. However, it is also important to consider the alternative hypothesis that clap-and-fling occurs as a concomitant byproduct of insects trying to maximize their stroke amplitude. For a given stroke frequency, maximizing stroke amplitude increases wing velocity. Since total flight forces are dependent on the square of wing velocity, an average 15° increase in stroke amplitude during steering behavior produces an increase in total lift of approximately 20% (Lehmann and Dickinson, 1997, 1998). Besides its role for total lift enhancement, a concomitant 10% lift augmentation due to clap-and-fling beneficially counterbalances pitch moments on the animal body produced by the increase in ventral stroke amplitude. Ultimately, this view is supported by high-speed video observations showing that in tethered flying *Drosophila* clap-and-fling wingbeat vanishes at small stroke amplitudes (low flight force production), whereas the tethered fly permanently uses clap-and-fling wing beat while producing elevated forces at stroke amplitudes near the mechanical limit of the thorax of 190° (Lehmann and Dickinson, 1998).

List of symbols

c	chord width
C_F	force coefficient
C_D	drag coefficient
C_L	lift coefficient
$\boldsymbol{g}(\theta)$	rotational coefficient
L	lift
n	stroke frequency
R	wing length
S	total wing area
$\hat{t}$	non-dimensional time
T	stroke period
t	time from the start of the downstroke
Φ	stroke amplitude
Γ_f	final circulation during fling motion for one wing
θ	angular distance
ρ	density
ω	angular rate of change of incidence of a single wing

We would like to acknowledge Don Pick for his help with DPIV imaging. This work was funded by NSF (IBN-0217229) and Packard Foundation grants to M.H.D., DFG grant Le 905/4-1 and German Federal Ministry for Education and Research (BMBF) grant Biofuture 0311885 to F.O.L.

References

Bennett, L. (1977). Clap and fling aerodynamics – an experimental evaluation. *J. Exp. Biol.* **69**, 261-272.

Birch, J. M. and Dickinson, M. H. (2001). Spanwise flow and the attachment of the leading-edge vortex on insect wings. *Nature* **412**, 729-733.

Birch, J. M. and Dickinson, M. H. (2003). The influence of wing–wake interactions on the production of aerodynamic forces in flapping flight. *J. Exp. Biol.* **206**, 2257-2272.

Brackenbury, J. (1990). Wing movements in the bush cricket *Tettigonia viridissima* and the mantis *Ameles spallanziana* during natural leaping. *J. Zool. Lond.* **220**, 593-602.

Brackenbury, J. (1991a). Kinematics of take-off and climbing flight in butterflies. *J. Zool. Lond.* **224**, 251-270.

Brackenbury, J. (1991b). Wing kinematics during natural leaping in the mantids *Mantis religiosa* and *Iris oratoria*. *J. Zool. Lond.* **223**, 341-356.

Brodsky, A. K. (1991). Vortex formation in the tethered flight of the peacock butterfly *Inachis io* L. (Lepidoptera, Nymphalidae) and some aspects of insect flight evolution. *J. Exp. Biol.* **161**, 77-95.

Cooter, R. J. and Baker, P. S. (1977). Weis-Fogh clap and fling mechanism in *Locusta*. *Nature* **269**, 53-54.

Dalton, S. (1975). *Borne On The Wind*. New York: Reader's Digest Press.
Dickinson, M. H. (1994). The effects of wing rotation on unsteady aerodynamic performance at low Reynolds numbers. *J. Exp. Biol.* **192**, 179-206.
Dickinson, M. H. and Götz, K. G. (1993). Unsteady aerodynamic performance of model wings at low Reynolds numbers. *J. Exp. Biol.* **174**, 45-64.
Dickinson, M. H., Lehmann, F.-O. and Sane, S. (1999). Wing rotation and the aerodynamic basis of insect flight. *Science* **284**, 1954-1960.
Edwards, R. H. and Cheng, H. K. (1982). The separation vortex in the Weis-Fogh circulation-generation mechanism. *J. Fluid Mech.* **120**, 463-473.
Ellington, C. P. (1975). Non-steady-state aerodynamics of the flight of *Encarsia formosa*. In *Symposium on Swimming and Flying in Nature* (ed. T. Y. Wu), pp. 729-762. Passadena: California.
Ellington, C. P. (1984a). The aerodynamics of insect flight. III. Kinematics. *Phil. Trans. R. Soc. Lond. B* **305**, 41-78.
Ellington, C. P. (1984b). The aerodynamics of insect flight. IV. Aerodynamic mechanisms. *Phil. Trans. R. Soc. Lond. B* **305**, 79-113.
Ellington, C. P. (1984c). The aerodynamics of insect flight. VI. Lift and power requirements. *Phil. Trans. R. Soc. Lond. B* **305**, 145-181.
Ellington, C. P. (1984d). The aerodynamics of insect flight. II. Morphological parameters. *Phil. Trans. R. Soc. Lond. B* **305**, 17-40.
Ellington, C. P., Berg, C. V. D., Willmott, A. P. and Thomas, A. L. R. (1996). Leading-edge vortices in insect flight. *Nature* **384**, 626-630.
Ennos, A. R. (1989). The kinematics and aerodynamics of the free flight of some Diptera. *J. Exp. Biol.* **142**, 49-85.
Fry, S. N., Sayaman, R. and Dickinson, M. H. (2003). The aerodynamics of free-flight maneuvers in *Drosophila*. *Science* **300**, 495-498.
Götz, K. G. (1987). Course-control, metabolism and wing interference during ultralong tethered flight in *Drosophila melanogaster*. *J. Exp. Biol.* **128**, 35-46.
Lehmann, F.-O. (1994). Aerodynamische, kinematische und electrophysiologische Aspekte der Flugkrafterzeugung und Flugkraftsteuerung bei der Taufliege *Drosophila melanogaster*. PhD thesis, University of Tübingen, Germany.
Lehmann, F.-O. (2002). The constraints of body size on aerodynamics and energetics in flying fruit flies: an integrative view. *Zoology* **105**, 287-295.
Lehmann, F.-O. (2004). The mechanisms of lift enhancement in insect flight. *Naturwissenschaften* **91**, 101-122.
Lehmann, F.-O. and Dickinson, M. H. (1997). The changes in power requirements and muscle efficiency during elevated force production in the fruit fly, *Drosophila melanogaster*. *J. Exp. Biol.* **200**, 1133-1143.
Lehmann, F.-O. and Dickinson, M. H. (1998). The control of wing kinematics and flight forces in fruit flies (*Drosophila* spp.). *J. Exp. Biol.* **201**, 385-401.
Lighthill, M. J. (1973). On the Weis-Fogh mechanism of lift generation. *J. Fluid Mech.* **60**, 1-17.
Marden, J. H. (1987). Maximum lift production during take-off in flying animals. *J. Exp. Biol.* **130**, 235-258.
Maxworthy, T. (1979). Experiments on the Weis-Fogh mechanism of lift generation by insects in hovering flight Part 1. Dynamics of the 'fling'. *J. Fluid Mech.* **93**, 47-63.
Maybury, W. J. and Lehmann, F.-O. (2004). The fluid dynamics of flight control by kinematic phase lag variation between two robotic insect wings. *J. Exp. Biol.* **207**, 4707-4726.
Miller, L. A. and Peskin, C. S. (2004). When vortices stick: an aerodynamic transition in tiny insect flight. *J. Exp. Biol.* **207**, 3073-3088.
Miller, L. A. and Peskin, C. S. (2005). A computational fluid dynamics of 'clap and fling' in the smallest insects. *J. Exp. Biol.* **208**, 195-212.
Noca, F., Shiels, D. and Jeon, D. (1999). A comparison of methods for evaluating time-dependent fluid dynamic forces on bodies, using only velocity fields and their derivatives. *J. Fluids Struct.* **13**, 551-578.
Ramamurti, R. and Sandberg, W. C. (2001). Computational study of 3-D, flapping foil, flows. *AIAA-2001,* 605.
Rosen, M. W., Spedding, G. R. and Hedenström, A. (2004). The relationship between wingbeat kinematics and vortex wake of a thrush nightingale. *J. Exp. Biol.* **207**, 4255-4268.
Sane, S. (2003). The aerodynamics of insect flight. *J. Exp. Biol.* **206**, 4191-4208.
Sane, S. and Dickinson, M. H. (2001). The control of flight force by a flapping wing: lift and drag production. *J. Exp. Biol.* **204**, 2607-2626.
Spedding, G. R. (2003). Comparing fluid mechanics models with experimental data. *Phil. Trans. R. Soc. Lond. B* **358**, 1567-1576.
Spedding, G. R. and Maxworthy, T. (1986). The generation of circulation and lift in a rigid two-dimensional fling. *J. Fluid Mech.* **165**, 247-272.
Spedding, G. R., Hedenström, A. and Rosen, M. W. (2003a). Quantitative studies of the wakes of freely flying birds in a low-turbulence wind tunnel. *Exp. Fluids* **34**, 291-303.
Spedding, G. R., Rosen, M. W. and Hedenström, A. (2003b). A family of vortex wakes generated by a thrush nightingale in free flight in a wind tunnel over its entire natural range of flight speeds. *J. Exp. Biol.* **206**, 2313-2344.
Srygley, R. B. and Thomas, A. L. R. (2002). Unconventional lift-generating mechanisms in free-flying butterflies. *Nature* **420**, 660-6604.
Sun, M. and Yu, X. (2003). Flows around two airfoils performing fling and subsequent translation and translation and subsequent clap. *Acta Mech. Sinica* **19**, 103-117.
Sunada, S., Kawachi, K., Watanabe, I. and Azuma, A. (1993). Fundamental analysis of three-dimensional 'near fling'. *J. Exp. Biol.* **183**, 217-248.
Usherwood, J. R. and Ellington, C. P. (2002). The aerodynamic of revolving wings. I. Model hawkmoth wings. *J. Exp. Biol.* **205**, 1547-1564.
Vogel, S. (1966). Flight in *Drosophila.* I. Flight performance of tethered flies. *J. Exp. Biol.* **44**, 567-578.
Wagner, H. (1925). Über die Entstehung des dynamischen Auftriebes von Tragflügeln. *Z. Angew. Math. Mech.* **5**, 17-35.
Wakeling, J. M. and Ellington, C. P. (1997). Dragonfly flight. II. Velocities, accelerations, and kinematics of flapping flight. *J. Exp. Biol.* **200**, 557-582.
Weis-Fogh, T. (1973). Quick estimates of flight fitness in hovering animals, including novel mechanisms for lift production. *J. Exp. Biol.* **59**, 169-230.
Weis-Fogh, T. (1974). In *Swimming and Flying in Nature*, vol. 2 (ed. Y. T. Wu, C. J. Brokaw and C. Brennen), pp. 729-762. New York: Plenum Press.
Wu, J. H. and Sun, M. (2004). Unsteady aerodynamic forces of a flapping wing. *J. Exp. Biol.* **207**, 1137-1150.
Wu, J. Z., Vakili, A. D. and Wu, J. M. (1991). Review of the physics of enhancing vortex lift by unsteady excitation. *Prog. Aerosp. Sci.* **28**, 73-131.
Zanker, J. M. (1990a). The wing beat of *Drosophila melanogaster.* I. Kinematics. *Phil. Trans. R. Soc. Lond. B* **327**, 1-18.
Zanker, J. M. (1990b). The wing beat of *Drosophila melanogaster.* III. Control. *Phil. Trans. R. Soc. Lond. B* **327**, 45-64.